Research Square

Preprints are preliminary reports that have not undergone peer review.
They should not be considered conclusive, used to inform clinical practice,
or referenced by the media as validated information.

Bclaf1 sustains the contractile phenotype of vascular smooth muscle cells to restrain neointimal hyperplasia in mice

Zhenwei Pan

panzw@ems.hrbmu.edu.cn

Harbin Medical University https://orcid.org/0000-0002-1011-0954

Chenhong Li

Harbin Medical University

Jialiang Li

Harbin Medical University

Yuying Zeng

Harbin Medical University

Zhiwen Zhou

Harbin Medical University

Chunxin You

Harbin Medical University

Ying Yang

Harbin Medical University

Shuang Wang

Harbin Medical University

Kaile Wang

Harbin Medical University

Zaiyi Yang

Harbin Medical University

Deli Zhao

Harbin Medical University

Yanjie Lu

Harbin Medical University

Yang Zhang

Harbin Medical University

Article

Keywords: vascular smooth muscle cells, phenotypic switching, cell proliferation, neointimal hyperplasia

Posted Date: November 19th, 2026

DOI: https://doi.org/10.21203/rs.3.rs-11601453/v1

License: This work is licensed under a Creative Commons Attribution 4.0 International License.
Read Full License

Additional Declarations: There is no duality of interest

Abstract

Inhibiting aberrant phenotypic switching and excessive proliferation of vascular smooth muscle cells (VSMCs) represents a promising therapeutic strategy for mitigating vascular restenosis and neointimal hyperplasia. Bclaf1 (Bcl-2-associated transcription factor 1) has emerged as a critical regulator of cellular homeostasis and phenotypic plasticity through the modulation of multiple downstream signaling networks. In this study, we demonstrate that Bclaf1 deletion exacerbates VSMC dedifferentiation, proliferation, and migration, thereby aggravating neointimal hyperplasia after arterial injury in mice. Conversely, smooth muscle cell-specific overexpression of Bclaf1 markedly attenuated neointimal lesion formation, preserved the contractile phenotype of VSMCs, and suppressed pathological vascular remodeling in murine models of vascular injury. Mechanistic analyses and functional rescue assays revealed that Bclaf1 maintains the contractile phenotype of VSMCs through two complementary mechanisms: stabilization of the Nexilin-mediated cytoskeleton and suppression of proliferation via the Rbm47–p53–p21 signaling axis. Restoration of Nexilin or activation of p53–p21 signaling substantially rescued the aberrant VSMC phenotype and excessive neointimal growth induced by Bclaf1 deficiency. Collectively, our findings identify Bclaf1 as a protective regulator of neointimal hyperplasia that sustains VSMC homeostasis through the Nexilin cytoskeletal pathway and the Rbm47–p53–p21 signaling cascade. These results reveal a previously unrecognized regulatory mechanism underlying vascular remodeling and highlight Bclaf1 as a potential therapeutic target for proliferative vascular diseases.

Introduction

Phenotypic switching of vascular smooth muscle cells (VSMCs) from a quiescent, contractile state to a proliferative, migratory, and synthetic phenotype is a central pathological driver of neointimal hyperplasia, atherosclerosis, and post-angioplasty restenosis[1–3]. In healthy vessels, differentiated VSMCs stably express contractile markers including myosin heavy chain 11 (Myh11), α-smooth muscle actin (Acta2), calponin 1 (Cnn1) and smoothelin, thereby maintaining vascular tone and structural homeostasis[4]. Transforming growth factor-β (TGF-β) is a key cytokine that sustains the contractile phenotype by activating Smad-dependent transcriptional programs and upregulating contractile gene expression[5]. Upon vascular injury, activated inflammatory cells, platelets, and VSMCs secrete multiple growth factors that profoundly reshape VSMC phenotype, suppressing contractile gene expression and upregulating synthetic markers including fibronectin 1 (Fn1), collagen type I alpha 1 chain (Col1a1), matrix metalloproteinase 9 (Mmp9) and secreted phosphoprotein 1 (Spp1). Among these factors, platelet-derived growth factor-BB (PDGF-BB) is the most potent and well-characterized inducer of VSMC phenotypic switching[6]. Although a large body of work has defined critical extracellular cues and downstream signaling cascades driving VSMC phenotypic reprogramming, the endogenous transcriptional mechanisms that preserve the contractile phenotype and restrain pathological VSMC plasticity remain incompletely defined.

Notably, single-cell RNA sequencing studies identify Bclaf1 as an activated transcription factor in contractile SMCs, with high expression in healthy arterial VSMCs that gradually diminishes as cells adopt

disease-related phenotypes[7]. Bcl-2-associated transcription factor 1 (Bclaf1) is a multifunctional nuclear protein with established roles in transcriptional control, pre-mRNA processing, DNA-damage response, and cellular stress signaling. Previous studies have demonstrated that Bclaf1 can cooperate with nuclear co-regulators such as p85β to modulate gene transcription. It also forms complexes with THRAP3 to orchestrate selective mRNA splicing and nuclear export upon DNA damage. Moreover, Bclaf1 participates in DNA-damage-triggered cellular senescence by acting as an NF-κB signal transducer and modulating C/EBPβ-dependent transcriptional programs[8–10].

Recent mechanistic studies further establish Bclaf1 as a chromatin-associated transcriptional regulator: it participates in super-enhancer-driven activation of POLR2A and remodels global chromatin accessibility during nitrosamine-driven esophageal carcinogenesis[11]. In cardiomyocytes, recent work further demonstrates that Bclaf1 acts as an RNA-splicing regulator. By interacting with splicing factor Srsf2, elevated Bclaf1 enhances Hand2 pre-mRNA maturation and drives maladaptive cardiac hypertrophy and heart failure[12]. Our previous work demonstrated that Bclaf1 modulates p53-dependent apoptosis in cardiomyocytes and exacerbates pathological cardiac remodeling[13]. Despite these advances across multiple cell types and disease models, whether Bclaf1 participates in the transcriptional control of VSMC fate and injury-provoked neointimal formation remains entirely unexplored. Given its documented ability to govern transcription and interact with nucleic-acid-associated regulatory complexes, we hypothesized that Bclaf1 functions as an upstream transcriptional regulator to stabilize the contractile VSMC phenotype.

Here, we demonstrate that Bclaf1 deficiency promotes VSMC phenotypic switching, proliferation, migration, and neointimal hyperplasia, whereas Bclaf1 overexpression suppresses these pathological responses. Mechanistically, Bclaf1 directly binds to regulatory regions of *Nexn* and *Rbm47*. *Nexn* encodes Nexilin, an F-actin-binding protein required for cytoskeletal integrity; Rbm47 in turn activates the p53–p21 axis to constrain excessive VSMC proliferation. Through coordinated regulation of these two targets, Bclaf1 preserves VSMC homeostasis and limits pathological vascular remodeling. Collectively, these findings identify Bclaf1 as a previously unrecognized transcriptional regulator of VSMC plasticity and point to its potential as a therapeutic target for neointimal hyperplasia and proliferative vascular diseases.

Materials and Methods

More detailed methods are described in the Supplementary Materials.

Experimental animals

Adult male C57BL/6 mice aged 8 weeks were used in this study. Mice were housed under controlled conditions with a 12 h light/dark cycle, a temperature of 23 ± 3°C, and humidity of 30–70%. Eight-week-old male mice were purchased from Cyagen Biosciences Company, China, and mice weighing 23 ± 2 g were selected for experiments. All animal procedures were approved by the Ethics Committee of Harbin

Medical University and were performed in accordance with the US National Institutes of Health Guide for the Care and Use of Laboratory Animals. Mice were randomly assigned to experimental groups using a computer-generated randomization scheme.

Generation of smooth muscle cell-specific Bclaf1 conditional knockout mice

Bclaf1$^{fl/fl}$ mice were generated by Cyagen Biosciences Inc. using CRISPR/Cas9-mediated genome editing. Smooth muscle cell-specific *Bclaf1* conditional knockout mice (Bclaf1 cKO) were generated by crossing Bclaf1$^{fl/fl}$ mice with Tagln-Cre transgenic mice. Bclaf1$^{fl/fl}$ littermates were used as controls. Genotyping was performed by PCR using genomic DNA from tail biopsies. Primer sequences are listed in **Supplementary Table 1**.

Isolation and culture of mouse vascular smooth muscle cells

Primary mouse aortic vascular smooth muscle cells were isolated from 8-week-old SPF mice. The aorta from the abdominal aorta to the aortic arch was excised under sterile conditions. Surrounding tissues and adventitia were removed under a stereomicroscope, and the medial layer was digested with type II collagenase (17101015, Gibco, Thermo Fisher Scientific, Waltham, MA, USA). Cells were cultured in DMEM/F12 medium (C3130-0500, VivaCell Biosciences, Shanghai, China) supplemented with fetal bovine serum (C04001-500, VivaCell Biosciences, Shanghai, China) and were identified by immunofluorescence staining for smooth muscle-specific markers. MOVAS cells and primary mouse vascular smooth muscle cells were used for in vitro experiments.

Cell proliferation, migration, and contraction assays

Cell proliferation was assessed using EdU incorporation assays (KTA2031, Abbkine, Atlanta, GA, USA). EdU-positive cells were quantified from at least five randomly selected fields per sample. Cell migration was evaluated using scratch wound assays, and wound closure was quantified using ImageJ. VSMC contractile function was assessed using a collagen gel contraction assay according to the manufacturer's instructions (CBA-5020, Cell Biolabs, San Diego, CA, USA).

Immunofluorescence staining

Mouse arterial sections, MOVAS cells, and primary mouse vascular smooth muscle cells were fixed with 4% formaldehyde and blocked with normal goat serum. Samples were incubated with primary antibodies against Bclaf1, Acta2, Nexilin or Flag, followed by fluorescent secondary antibodies. F-actin and nuclei were stained with phalloidin and DAPI (C1006, Beyotime Biotechnology, Shanghai, China), respectively.

Images were acquired using a confocal fluorescence microscope. Antibody information is provided in **Supplementary Table 2**.

AAV9-mediated Bclaf1 overexpression

Bclaf1 overexpression virus was constructed using the CRISPR/Cas9 system by Cyagen Biosciences (Guangzhou, China). For smooth muscle cell-targeted Bclaf1 overexpression, an AAV9 vector encoding Bclaf1 under the control of the SM22α promoter was generated and designated AAV9-Bclaf1. An empty Flag-tagged vector was used as the negative control (AAV9-NC). The virus was injected into 6-week-old C57BL/6 mice through the tail vein at a dose of 1×10^{13} genome copies per animal. Experimental interventions were performed 2 weeks after viral injection.

Mouse carotid artery wire injury

Eight-week-old male C57BL/6J mice were anesthetized with tribromoethanol at 100 mg/kg by intraperitoneal injection. The left common carotid artery, left internal carotid artery, and left external carotid artery were exposed under a stereomicroscope. A 0.34 mm guide wire was inserted through the external carotid artery and advanced into the common carotid artery to induce intimal injury by friction. After injury, blood flow was restored, and the skin incision was closed. Sham-operated mice underwent the same surgical exposure without guide wire insertion or intimal injury.

Western blotting

Proteins were extracted from vascular tissues or cultured cells, separated by SDS-PAGE, and transferred to nitrocellulose membranes. Membranes were incubated with primary antibodies against Bclaf1, Acta2, Cnn1, Myh11, Smoothelin, Fn1, Col1a1, Spp1, Mmp9, Nexilin, Rbm47, p53, p21, or β-tubulin, followed by fluorescence-conjugated secondary antibodies. Signals were detected using an Odyssey infrared imaging system (LI-COR Biosciences, Lincoln, NE, USA). Antibody information is provided in **Supplementary Table 2**.

Quantitative real-time PCR

Total RNA was extracted from MOVAS cells and primary mouse vascular smooth muscle cells using TRIzol reagent (15596026, Invitrogen, Carlsbad, CA, USA). RNA was reverse transcribed into cDNA using a first-strand cDNA synthesis kit (AT341-02, TransGen Biotech, Beijing, China). Quantitative PCR was performed using TransStart Top Green qPCR SuperMix (AQ131-02, TransGen Biotech, Beijing, China). Relative mRNA expression was normalized to β-actin and calculated using the comparative Ct method. Primer sequences are listed in **Supplementary Table 3**.

Statistical analysis

Data are presented as mean ± SEM. Statistical analyses were performed using GraphPad Prism 9. Comparisons between two groups were performed using two-tailed unpaired Student's t-tests. Comparisons among multiple groups were performed using one-way ANOVA followed by Tukey's multiple comparison test. Two-way ANOVA followed by Bonferroni's post hoc test was used for experiments involving two independent variables. $P < 0.05$ was considered statistically significant.

Results

Bclaf1 Expression Correlates with Neointima Formation and Coordinates with Contractile Proteins in Intimal Hyperplasia

To investigate dynamic changes in Bclaf1 expression during neointimal hyperplasia, we established a mouse carotid artery wire injury model[14], a widely used preclinical model that recapitulates the transition of VSMCs from a contractile phenotype to a proliferative and synthetic state[15, 16]. We examined Bclaf1 expression in the developing neointima at 14 and 28 days after injury. Immunofluorescence staining showed that Bclaf1 and the contractile marker Acta2 were progressively downregulated over time, in parallel with neointima formation (Fig. 1A). Complementary western blot analysis of carotid artery tissue lysates collected at 28 days post-injury further confirmed the coordinated reduction of Bclaf1 alongside multiple contractile proteins, including Myh11, Smoothelin, Acta2, and Cnn1, in injured arteries relative to sham controls (Fig. 1B). Additional immunofluorescence analysis revealed a striking cell cycle-dependent subcellular localization pattern of Bclaf1 in VSMCs. During interphase, Bclaf1 localized predominantly to the nucleus. Upon mitotic entry, Bclaf1 was excluded from condensed chromosomes and redistributed diffusely throughout the cytoplasm. This dynamic localization pattern indicates that Bclaf1 is an interphase-enriched nuclear protein whose subcellular distribution is tightly coupled to cell cycle progression (Fig. 1C).

In cultured mouse aortic smooth muscle cells (MOVAS), treatment with TGF-β, a well-characterized positive regulator of VSMC differentiation, significantly upregulated the mRNA levels of Bclaf1 and the contractile markers Myh11, Smoothelin, Acta2, and Cnn1 (Fig. 1D). Conversely, treatment with PDGF-BB, the most potent inducer of VSMC dedifferentiation, resulted in synchronous downregulation of Bclaf1 and the full panel of contractile marker mRNAs (Fig. 1E). Consistent with these transcriptional changes, TGF-β treatment significantly increased the protein levels of Bclaf1, Myh11, Smoothelin, Acta2, and Cnn1 compared with vehicle-treated controls (Fig. 1F). In contrast, PDGF-BB treatment markedly reduced the protein levels of Bclaf1 and the same panel of contractile markers (Fig. 1G). Collectively, these in vivo and in vitro data demonstrate that Bclaf1 expression is closely associated with the VSMC phenotypic state, supporting a potential regulatory role for Bclaf1 in maintaining the contractile VSMC phenotype and restraining pathological neointimal hyperplasia.

Bclaf1 regulates VSMCs phenotypic switching in vitro

VSMCs exhibit remarkable phenotypic plasticity, ranging from a quiescent contractile state in mature arteries to a proliferative and synthetic state during neointimal hyperplasia [17, 18]. To define the functional role of Bclaf1 in VSMC phenotypic switching, we first knocked down Bclaf1 in MOVAS cells using small interfering RNA (siRNA). Knockdown efficiency was confirmed by Western blotting, and Bclaf1-Si2, which achieved the most robust knockdown, was selected for subsequent experiments **(**Fig. 2A, B**)**. Bclaf1 depletion significantly reduced both the mRNA and protein levels of a comprehensive panel of canonical VSMC contractile markers, including Myh11, Smoothelin, Acta2 and Cnn1 (Fig. 2C, D). Immunofluorescence staining further supported these findings, showing a marked decrease in the mean fluorescence intensity (MFI) of Acta2 in Bclaf1-deficient VSMCs (Fig. 2E). Functionally, collagen gel contraction assays demonstrated that Bclaf1 knockdown significantly impaired VSMC contractile capacity (Fig. 2F). We additionally assessed the expression of synthetic VSMC markers, including Fn1, Col1a1, Mmp9 and Spp1, and observed their coordinated upregulation following Bclaf1 silencing **(**Fig. 2G, H**)**. We next assessed the effects of Bclaf1 deficiency on VSMC proliferation and migration, two hallmark features of the synthetic phenotype. EdU incorporation assays revealed that Bclaf1 silencing markedly increased the proportion of proliferating VSMCs compared with control cells (Fig. 2I). In parallel, scratch wound assays showed that Bclaf1 knockdown significantly enhanced VSMC migratory capacity (Fig. 2J). Taken together, these loss-of-function data indicate that Bclaf1 deficiency promotes the transition of VSMCs from a contractile phenotype to a synthetic phenotype.

To corroborate these findings, we performed complementary gain-of-function experiments by overexpressing Bclaf1 in VSMCs. Efficient overexpression was verified by Western blotting (Fig. 2K). Consistent with the knockdown results, Bclaf1 overexpression significantly increased both the mRNA and protein levels of Myh11, Smoothelin, Acta2 and Cnn1 (Fig. 2L, M). Immunofluorescence staining confirmed increased Acta2 MFI in Bclaf1-overexpressing cells (Fig. 2N). Functionally, collagen gel contraction assays showed that Bclaf1 overexpression modestly enhanced VSMC contractile function (Fig. 2O). In line with the stabilization of the contractile program, Bclaf1 overexpression reduced the mRNA and protein abundance of synthetic markers Fn1, Col1a1, Mmp9 and Opn **(**Fig. 2P, Q**)**. Conversely, Bclaf1 overexpression significantly attenuated VSMC proliferation and migration, as measured by EdU incorporation and scratch wound assays, respectively (Fig. 2R, S).

To extend these findings to a more physiological system, we isolated primary mouse aortic smooth muscle cells (mVSMCs) from 8-week-old wild-type mice as previously described[19]. The key phenotypes observed in MOVAS cells were largely recapitulated in primary mVSMCs **(Fig. S1)**.

Collectively, these loss-of-function and gain-of-function studies, performed in both immortalized and primary VSMCs, support Bclaf1 as a regulator sustaining the contractile molecular signature of VSMCs. Loss of Bclaf1 promotes features of dedifferentiation, including enhanced proliferation, migration, and induction of synthetic-associated genes, whereas Bclaf1 overexpression restores or preserves contractile marker expression and limits proliferative and migratory activity.

Bclaf1 deficiency in VSMCs exacerbates post-injury neointima formation in mice

To determine the role of Bclaf1 in the phenotypic switching of VSMC cells and the development of pathological neointimal hyperplasia in vivo, we created Bclaf1 conditional knockout mice by crossing Bclaf1-floxed mice with Tagln-Cre transgenic mice (Fig. 3A). Western blot analysis confirmed specific and complete ablation of Bclaf1 in the aortic smooth muscle cells of Bclaf1 cKO mice relative to $Bclaf1^{fl/fl}$ littermates (Fig. 3B). Immunofluorescence staining of sections from the left common carotid artery and thoracic aorta revealed significantly reduced expression of the contractile marker Acta2 in Bclaf1 cKO mice compared to controls (Fig. 3C, D). Consistent with these imaging data, immunoblotting of aortic lysates demonstrated coordinated downregulation of the full panel of contractile proteins, including Myh11, Smoothelin, Acta2, and Cnn1, in Bclaf1-cKO vessels (Fig. 3E). We further detected concurrent upregulation of synthetic VSMC markers, including Fn1, Col1a1, Mmp9, and Spp1, in the aorta of Bclaf1-cKO mice (Fig. 3F). Under basal physiological conditions, hematoxylin and eosin staining revealed no significant differences in medial thickness, medial area, or overall vascular structure between the two genotypes (Fig. 3G).

To induce pathological vascular remodeling, $Bclaf1^{fl/fl}$ control mice and Bclaf1 cKO mice were subjected to unilateral carotid artery injury. The contralateral, uninjured carotid artery served as a control for each mouse. Vascular tissues were harvested at 14 and 28 days after injury for histological and quantitative morphometric analyses. Bclaf1 cKO mice developed significantly larger neointimal lesions and exhibited more pronounced intimal thickening compared to $Bclaf1^{fl/fl}$ control mice at both time points (Fig. 3H). Together, these in vivo data align with our in vitro results and show that smooth muscle-specific Bclaf1 loss shifts the molecular profile of VSMCs away from the contractile signature toward a synthetic program and aggravates injury-triggered neointimal hyperplasia.

Bclaf1 overexpression attenuates neointima formation following carotid artery injury in mice

Having shown that smooth muscle cell-specific deletion of Bclaf1 exacerbates post-injury neointimal hyperplasia, we next performed complementary gain-of-function studies to determine whether Bclaf1 overexpression could protect against pathological vascular remodeling. To this end, we generated an SM22α promoter-driven adeno-associated virus serotype 9 (AAV9) vector for smooth muscle cell-specific Bclaf1 overexpression (designated AAV9-Bclaf1), with an empty vector carrying the same Flag tag serving as the negative control (AAV9-NC). Age-matched male mice were administered AAV9-NC or AAV9-Bclaf1 by tail vein injection 14 days before unilateral carotid artery wire injury, and injured left common carotid arteries were harvested at 14 and 28 days after injury (Fig. 4A). Western blotting confirmed robust overexpression of Flag-tagged Bclaf1 in vascular tissues from AAV9-Bclaf1-treated mice (Fig. 4B). Immunofluorescence staining of thoracic aorta and carotid artery sections showed comparable Flag signal intensity in the medial smooth muscle layer between AAV9-NC- and AAV9-

Bclaf1-treated mice, consistent with the presence of the Flag tag in both viral vectors. Notably, Acta2 expression was significantly increased in both thoracic aortas and carotid arteries following Bclaf1 overexpression (Fig. 4C, D). Consistently, immunoblotting of vessel lysates demonstrated coordinated upregulation of the full panel of contractile proteins, including Myh11, Smoothelin, Acta2, and Cnn1, upon Bclaf1 overexpression **(**Fig. 4E**)**. We also observed concomitant downregulation of synthetic markers Fn1, Col1a1, Mmp9, and Spp1 in AAV9-Bclaf1 vessels **(**Fig. 4F**)**. Under basal uninjured conditions, hematoxylin and eosin (H&E) staining revealed no significant differences in medial thickness, medial area, or overall vascular architecture between AAV9-Bclaf1 and AAV9-NC mice (Fig. 4G).

Following unilateral carotid artery wire injury, with the contralateral uninjured carotid artery serving as an internal control for each mouse, carotid tissues were harvested at 14 and 28 days after injury for histological and quantitative morphometric analyses. H&E staining showed that AAV9-Bclaf1-treated mice developed significantly smaller neointimal lesions and exhibited less pronounced intimal thickening than AAV9-NC controls at both time points **(**Fig. 4H**)**.

Collectively, these *in vivo* gain-of-function data indicate that smooth muscle cell-specific overexpression of Bclaf1 promotes a contractile molecular signature in VSMCs and attenuates pathological neointimal hyperplasia after arterial injury, providing complementary evidence that Bclaf1 protects against vascular remodeling.

Bclaf1 directly controls Nexilin and Rbm47 transcription

VSMC phenotypic switching is governed by a complex network of growth factors, actin cytoskeletal dynamics, cell cycle progression, and transcriptional regulators that together balance the contractile and synthetic states [20]. We first characterized the subcellular localization of Bclaf1 in VSMCs. Immunofluorescence staining showed that Bclaf1 localized predominantly to the nucleus in both MOVAS cells and primary mouse aortic smooth muscle cells, with a similar nuclear localization pattern observed in the medial layer of the left common carotid artery (LCCA) in vivo. Consistently, subcellular fractionation assays confirmed marked enrichment of Bclaf1 in the nuclear fraction (**Fig. S2A and S2B**). These findings support Bclaf1 as a nuclear protein in VSMCs, consistent with its proposed role in transcriptional regulation.

To define the global transcriptional program regulated by Bclaf1, we performed bulk RNA sequencing (RNA-seq) on primary aortic smooth muscle cells isolated from Bclaf1 cKO mice and Bclaf1 littermate controls (Fig. 5A). Transcriptional profiling revealed widespread gene expression changes in Bclaf1-deficient VSMCs, with 383 genes significantly upregulated and 373 genes significantly downregulated compared with control cells. Gene Ontology Biological Process (GO-BP) enrichment analysis showed that upregulated genes were enriched for terms related to vascular development and vascular diameter regulation (**Fig. S3A**), whereas downregulated genes were strongly associated with VSMC contractile function and actomyosin cytoskeletal organization (**Fig. S3B**). These transcriptomic data suggest that Bclaf1 regulates a transcriptional program essential for maintaining VSMC phenotypic stability.

We next performed chromatin immunoprecipitation sequencing (ChIP-seq) to identify direct genomic targets of Bclaf1 in mouse aortic smooth muscle cells. KEGG pathway enrichment analysis of Bclaf1-bound genomic regions revealed significant enrichment of genes involved in smooth muscle contraction and actin cytoskeleton regulation **(Fig. S3C)**. Integrated analysis of RNA-seq and ChIP-seq datasets identified 17 overlapping target genes. We identified key genes regulating VSMCs proliferation by analyzing overlapping genes between RNAseq and ChIPseq datasets and cell proliferation related genes, and this process generated five pivotal genes including *Rbm47*, *Tspan15*, *Adamts12*, *Ghr*, and *Nexn* (Fig. 5B). To identify the candidate genes potentially related to contractile phenotypic in VSMCs, we initially analyzed 2 data sets, VSMCs contractile phenotype-related genes[21] and differentially expressed markers for contractile VSMCs[22], to screen for critical genes that are both involved in VSMCs contractile phenotypic and highly expressed in VSMCs. As shown by Venn diagram, Nexn and Plxdc2 were overlapped from the aforementioned 4 data sets and emerged as main candidate genes linking VSMCs contractile phenotypic switching (Fig. 5C). We next visualized the expression changes of the candidate genes in the RNA-seq volcano plot. Consistent with contractile phenotypic switching, Bclaf1 and canonical contractile markers, including Acta2, Cnn1, and Tagln, were significantly downregulated **(**Fig. 5D**)**. The qRT-PCR verification showed that *Nexn* and *Rbm47* were significantly downregulated, whereas *Tspan15, Adamts12, Ghr* and *Plxdc2* had no obvious expression change (Fig. 5E). *Nexn* encodes Nexilin, an F-actin-binding protein that is important for maintaining cytoskeletal integrity. The dynamic equilibrium between globular actin (G-actin) and filamentous actin (F-actin) directly modulates downstream signaling pathways and transcriptional programs linked to VSMC differentiation and proliferation[23, 24]. *Rbm47* encodes an RNA-binding protein previously shown to enhance p53 promoter activity, thereby upregulating p53 and its downstream target p21 to induce cell cycle arrest or senescence[25]. These known functions are consistent with the phenotypic changes observed in Bclaf1-deficient VSMCs.

To establish direct regulation, we mapped Bclaf1 binding sites in these two targets. ChIP-seq analysis demonstrated that Bclaf1 specifically binds to intronic regions of both *Nexn* and *Rbm47* **(Fig. S3D)**. Notably, Bclaf1 occupancy was not detected within the 2000 bp region upstream of the transcription start site (TSS), the canonical core promoter region, suggesting that Bclaf1 may regulate these genes through distal regulatory elements. ChIP-qPCR using locus-specific primers confirmed robust Bclaf1 enrichment at the identified *Nexn* intronic region (Fig. 5F). To assess the enhancer activity of this binding region, we cloned the N1 motif containing smaller E1 and E3 fragments into the pGL3-Promoter vector. Luciferase reporter assays showed that constructs carrying the N1 motif exhibited significantly higher transcriptional activity than the empty vector control, with a 1.5-fold increase in promoter activity (Fig. 5G). To further determine whether Bclaf1 directly activates *Nexn* transcription through this enhancer, we generated reporter plasmids containing the *Nexn* promoter alone or in combination with the N1 enhancer. Luciferase assays showed that Bclaf1 co-expression significantly increased reporter activity only in the presence of the N1 enhancer (Fig. 5H). These data indicate that Bclaf1 promotes *Nexn* transcription by binding to its intronic enhancer region.

We performed analogous experiments to characterize Bclaf1-mediated regulation of *Rbm47*. Interrogation of public H3K4me3 ChIP-seq data using the Cistrome Data Browser confirmed the predicted promoter region of *Rbm47* and identified additional potential Bclaf1-binding sites within this region (Fig. 5I). ChIP-qPCR validation confirmed prominent Bclaf1 enrichment at the *Rbm47* promoter as well as at the distal E4 and E5 enhancer fragments (Fig. 5J). Luciferase reporter assays demonstrated that both E4 and E5 fragments possessed intrinsic enhancer activity (Fig. 5K). Furthermore, Bclaf1 overexpression significantly enhanced the transcriptional activity of the *Rbm47* promoter alone (Fig. 5L), and this effect was further increased when the promoter was combined with both the E4 and E5 enhancer sequence (Fig. 5M). These data indicate that Bclaf1 positively regulates *Rbm47* transcription by occupying both its promoter and distal enhancer regions.

Sequence alignment of Bclaf1-bound regions revealed high homology between the N1 motif in the *Nexn* locus and the R1 motif in the *Rbm47* locus, both of which overlapped with the strongest Bclaf1 ChIP-seq peaks. Motif analysis using the MEME Suite further identified a consensus Bclaf1-binding sequence present in all three validated regulatory regions, including the *Rbm47* promoter, *Rbm47* enhancer, and *Nexn* enhancer (Fig. 5N).

Given the reported interaction between Bclaf1 and HIF1α in hypoxic tumour models[26–28], we examined whether Bclaf1 controls Hif1α expression or directly occupies the Hif1a locus in normoxic VSMCs **(Fig. S4A-B)**. Neither knockdown nor overexpression of Bclaf1 altered Hif1a mRNA or Hif1α protein levels **(Fig. S4C-F)**. These results indicate that Bclaf1 regulates VSMC phenotypic switching independent of HIF1α signalling under normoxic conditions.

We further validated these findings *in vivo*. Immunofluorescence staining showed that the expression of both Nexilin and Rbm47 was markedly reduced in the vascular smooth muscle layer of Bclaf1 cKO mice compared with Bclaf1$^{fl/fl}$ littermate controls (Fig. 5O, P). Reciprocally, systemic overexpression of Bclaf1 via AAV9 delivery in wild-type mice robustly elevated the protein abundance of Nexilin and Rbm47 in vascular tissues, as confirmed by immunoblotting and quantitative densitometric analysis **(Fig. S5A, B)**. Consistent with the in vivo data, Bclaf1 knockdown in MOVAS cells significantly reduced the protein expression of Nexilin and Rbm47 **(**Fig. 5Q, R**)**, whereas Bclaf1 overexpression significantly increased their mRNA and protein levels (Fig. 5S-U). Similar results were obtained in primary mouse aortic smooth muscle cells (**Fig. S6**).

Collectively, these multi-omic and functional data demonstrate that Bclaf1 directly binds to regulatory elements in the *Nexn* and *Rbm47* loci and promotes their transcription. Nexn maintains VSMC contractile function by stabilizing the actin cytoskeleton, whereas Rbm47 restricts VSMC proliferation by activating the p53–p21 cell cycle checkpoint pathway. Through coordinated regulation of these two targets, Bclaf1 preserves VSMC phenotypic homeostasis and limits pathological vascular remodeling.

Overexpression of Nexilin or Rbm47 partially reverses VSMCs phenotypic switching induced by Bclaf1 deficiency

We next dissected the specific role of Nexilin in mediating Bclaf1-dependent regulation of VSMC phenotypic switching. The actin cytoskeleton provides a fundamental scaffold that governs VSMC morphology, mechanical properties, and phenotypic identity[29, 30]. Nexilin is an F-actin-binding protein that plays an important role in cytoskeletal organization and stabilization. Dysregulation of actin cytoskeletal architecture disrupts VSMC quiescence and promotes dedifferentiation, yet the upstream transcriptional regulators that maintain cytoskeletal homeostasis in VSMCs remain poorly characterized.

We first investigated whether Nexilin directly modulates VSMC phenotypic switching. Western blotting confirmed efficient overexpression of Nexilin in MOVAS cells (Fig. 6A). Nexilin overexpression significantly increased the protein levels of the full panel of canonical contractile markers, including Myh11, Smoothelin, Acta2, and Cnn1 (Fig. 6B), while reducing the abundance of synthetic markers Fn1, Col1a1, Mmp9, and Spp1 (Fig. 6C). EdU incorporation assays showed that Nexilin overexpression markedly suppressed VSMC proliferation (Fig. 6D). Consistent with these findings, scratch wound healing assays showed that Nexilin overexpression significantly reduced VSMC migratory capacity (Fig. 6E). We then performed rescue experiments to determine whether Nexilin mediates the effects of Bclaf1 on the VSMC phenotype. VSMCs were co-transfected with control or Bclaf1 siRNA together with empty vector or Nexilin overexpression plasmids. Nexilin overexpression partially restored the expression of contractile markers (Myh11, Smoothelin, Acta2, and Cnn1) and attenuated the upregulation of synthetic markers (Fn1, Col1a1, Mmp9, and Spp1) upon Bclaf1 knockdown, although these molecular parameters were not fully rescued to the levels seen in control VSMCs (Fig. 6F, G). Phalloidin staining, which labels filamentous actin (F-actin), showed that Nexilin overexpression enhanced F-actin polymerization and restored the F-actin/G-actin ratio in Bclaf1-silenced VSMCs (Fig. 6H). Functionally, EdU incorporation and scratch wound healing assays demonstrated that Nexilin overexpression significantly attenuated the increased proliferation and migration of VSMCs caused by Bclaf1 deficiency (Fig. 6I, J). Collectively, these data indicate that Nexilin acts as a key downstream effector of Bclaf1, supporting the contractile molecular signature of VSMCs by stabilizing the actin cytoskeleton and restraining synthetic phenotype-associated proliferation and migration.

Having identified Nexilin as a key downstream effector of Bclaf1, we next characterized the functional role of Rbm47 and its canonical downstream mediators p53 and p21. Efficient overexpression of Rbm47 was confirmed by Western blotting in MOVAS cells (Fig. 7A). Rbm47 overexpression significantly increased the protein levels of p53 and its direct downstream target p21 (Fig. 7B, C). EdU incorporation assays further showed that Rbm47 overexpression markedly suppressed VSMC proliferation (Fig. 7D). These data indicate that Rbm47 acts as a negative regulator of VSMC proliferation. We then performed rescue experiments to determine whether Rbm47 mediates the proliferative phenotype induced by Bclaf1 deficiency. VSMCs were co-transfected with control or Bclaf1 siRNA together with empty vector or Rbm47 overexpression plasmids. Rbm47 overexpression alone markedly increased p53 and p21 protein levels and rescued the reduction in p53 and p21 expression caused by Bclaf1 knockdown (Fig. 7E, F). Functional EdU assays confirmed that Rbm47 overexpression significantly attenuated VSMC hyperproliferation induced by Bclaf1 silencing (Fig. 7G). This rescue was restricted to the proliferative branch and failed to broadly reverse the full spectrum of VSMC phenotypic remodeling. Collectively,

these findings demonstrate that Rbm47 functions as another key downstream effector of Bclaf1, restricting VSMC proliferation by activating the p53–p21 cell cycle checkpoint pathway.

These results support that Nexilin and Rbm47 represent two complementary downstream effectors of Bclaf1. Nexilin partially rescues multiple features of VSMC remodeling upon Bclaf1 loss, whereas Rbm47 selectively restores p53–p21 signaling to mitigate excessive proliferation. The incomplete nature of these rescues further suggests that additional downstream regulators may contribute to the full spectrum of Bclaf1-controlled VSMC molecular phenotypes.

Discussion

Pathological phenotypic switching of VSMCs plays a central role in neointimal hyperplasia and restenosis following vascular intervention[31, 32]. In the present study, we demonstrate that Bclaf1 functions as a transcriptional regulator that supports the contractile molecular signature of VSMCs and restrains injury-induced neointimal formation. Loss of Bclaf1 shifts VSMC molecular profiles toward a synthetic state, accompanied by enhanced dedifferentiation, proliferation, and migration, whereas smooth muscle cell-specific overexpression of Bclaf1 counteracts these pathological changes and attenuates pathological vascular remodeling. Mechanistically, Bclaf1 exerts its protective effects through two complementary downstream targets, *Nexn* and *Rbm47*. Nexilin contributes broadly to sustaining VSMC contractile features by maintaining actin cytoskeletal integrity, whereas Rbm47 predominantly restrains aberrant proliferation via the p53–p21 axis. Notably, both rescue effects are only partial, indicating that additional downstream mediators likely participate in Bclaf1-dependent VSMC regulation. These findings reveal a previously unrecognized dual-layered regulatory role of Bclaf1 in linking cytoskeletal stability with cell cycle restraint in VSMCs.

VSMCs exhibit remarkable plasticity and can switch from a quiescent contractile phenotype to a proliferative synthetic phenotype under both physiological and pathological conditions. This phenotypic transition is triggered by diverse pathological stimuli and enables VSMCs to participate in vascular adaptation, repair, and remodeling [33–35]. Several epigenetic and transcriptional regulators have been implicated in this process. For example, PRMT5 epigenetically silences contractile gene expression through symmetric dimethylation of histone H3R8 and H4R3, reduces histone acetylation, and impairs SRF–myocardin–p300 recruitment to CArG elements, thereby promoting VSMC phenotypic switching and neointimal formation[36]. Single-cell RNA sequencing studies identify Bclaf1 as an activated transcription factor in contractile SMCs, with high expression in normal arterial VSMCs that progressively declines as cells acquire disease-associated phenotypes[7]. In line with these single-cell profiles, Bclaf1 is abundantly expressed in normal VSMCs but significantly downregulated in early atherosclerotic lesions[37]. While these correlative observations implied a homeostatic function for Bclaf1 in vascular biology, direct functional evidence was previously lacking. Consistent with these prior expression patterns, our study demonstrates that Bclaf1 is required for maintaining the contractile phenotype of VSMCs. Bclaf1 deficiency drives coordinated downregulation of contractile markers (Myh11, Smoothelin, Acta2 and Cnn1) and upregulation of synthetic markers (Fn1, Col1a1, Mmp9 and

Spp1), accelerating VSMC dedifferentiation, proliferation, and migration and ultimately exacerbating vascular stenosis. Conversely, Bclaf1 overexpression reverses this molecular shift and suppresses neointimal hyperplasia, a key pathological hallmark of occlusive vascular diseases.

Bclaf1 was initially identified as an adenoviral E1B19-binding protein with reported apoptosis-inducing and transcriptional regulatory activities[38]. In human fibroblasts, Bclaf1 inhibits human cytomegalovirus replication by repressing viral immediate-early gene transcription[39]. It also engages enhancer-associated transcriptional complexes to drive target gene expression in tumour cells[11]. We previously reported that Bclaf1 contributes to cardiac pathology by enhancing the transcriptional function of p53 during ischemia/reperfusion injury[13]. Together, these studies indicate that the biological functions of Bclaf1 are highly cell type-specific and context-dependent. In cardiomyocytes under ischemic stress, Bclaf1 promotes p53-mediated apoptosis. In VSMCs, our present study shows that Bclaf1 activates distinct transcriptional programs centered on *Nexn* and *Rbm47*, which bolster contractile gene expression or constrain cell cycle progression, respectively. Thus, Bclaf1 can generate divergent transcriptional outputs in different cardiovascular cell types, highlighting the complexity of its regulatory network.

Actin cytoskeleton remodeling is tightly coupled to VSMC contractile function and phenotypic stability[40]. During vascular contraction, F-actin content increases markedly in VSMCs. Cytoplasmic F-actin formation promotes MAL nuclear translocation after its dissociation from G-actin, thereby activating SRF-dependent contractile gene expression and sustaining the contractile phenotype[41]. Nexilin is an F-actin-binding protein essential for actin cytoskeletal stability and maintenance of the contractile apparatus[42]. Platelet-derived growth factor downregulates Nexilin through the Ras/Akt pathway. This reduction causes G-actin accumulation and F-actin loss in VSMCs, promoting their transition toward a synthetic phenotype[43]. Moreover, Nexilin silencing in VSMCs activates endoplasmic reticulum stress, accelerates cell cycle progression, and exacerbates post-injury neointimal hyperplasia[44]. Our data show that Bclaf1 directly binds to an intronic enhancer region of *Nexn* and promotes its transcription. Restoration of Nexilin expression substantially alleviates the dedifferentiation, hyperproliferation, and enhanced migration caused by Bclaf1 deficiency. These findings support a model in which Bclaf1 maintains VSMC contractile identity by sustaining Nexilin expression and preserving actin cytoskeletal integrity, which in turn stabilizes the SRF–MAL transcriptional axis.

In addition to cytoskeletal remodeling, aberrant cell cycle activation is a defining feature of synthetic VSMCs. The transition from the quiescent G0 phase to the G1/S phase marks the initiation of cell cycle progression and proliferative activation. p21, a classical transcriptional target of p53, functions as a broad-spectrum cyclin-dependent kinase inhibitor and plays a non-redundant role in restricting cell cycle progression [45]. Adenovirus-mediated overexpression of p21 inhibits VSMC proliferation and neointimal hyperplasia by blocking G1/S phase transition[46]. Rbm47 has been reported to directly activate the p53–p21 signaling axis at the transcriptional level, thereby promoting senescence and suppressing apoptosis in cancer cells following DNA damage[25]. Our study further shows that Bclaf1 directly binds to both the promoter and distal enhancer regions of *Rbm47* in VSMCs and enhances its transcription.

Subsequent upregulation of Rbm47 activates the p53–p21 axis, which in turn inhibits abnormal VSMC proliferation. Collectively, these findings indicate that Bclaf1 regulates VSMC proliferation through the Rbm47–p53–p21 cell cycle checkpoint pathway.

Notably, previous studies in hypoxic tumour systems have reported that Bclaf1 stabilizes HIF1α and promotes HIF1α-dependent angiogenesis. However, our data indicate that this regulatory axis is not operative in normoxic VSMCs. We observed no significant changes in *Hif1a* mRNA or HIF1α protein abundance upon Bclaf1 manipulation, and Bclaf1 ChIP-seq did not reveal obvious occupancy at the *Hif1a* locus. Thus, the function of Bclaf1 in VSMC phenotypic switching and neointimal suppression is independent of HIF1α signalling, and instead relies on its newly identified downstream targets Nexilin and Rbm47.

This study has some limitations. Although we demonstrate that Bclaf1 inhibits abnormal VSMC proliferation and neointimal hyperplasia in rodents, its translational relevance to human vascular proliferative diseases remains to be determined. Human vascular biology differs from that of rodents in cellular composition, extracellular matrix structure, and injury responses. Moreover, the potential crosstalk between the Nexilin–actin cytoskeleton pathway and the Rbm47–p53–p21 axis remains undefined. Given that cytoskeletal remodeling can influence the nuclear localization and activity of transcription factors, including p53, these two pathways may function in a coordinated manner. In addition, the partial rescue observed with Nexilin and Rbm47 implies that other Bclaf1 downstream effectors likely contribute to the overall VSMC molecular phenotype. The therapeutic potential of targeting Bclaf1 for intervention of vascular proliferative disorders in clinical practice also awaits further comprehensive investigation. Future studies employing large animal models and clinically relevant disease systems will help validate the translational value of targeting this axis.

In conclusion, our study identifies Bclaf1 as an important transcriptional regulator of the VSMC contractile phenotype and vascular homeostasis. By directly activating *Nexn* transcription to maintain actin cytoskeletal integrity and upregulating *Rbm47* to enforce p53–p21-dependent cell cycle restraint, Bclaf1 coordinately restrains the molecular shift toward a synthetic state and its associated cellular behaviours. This work describes two complementary downstream axes that contribute to Bclaf1 function, rather than defining a complete dual mechanism governing all facets of VSMC phenotypic plasticity. These findings identify Bclaf1 as a potential molecular target for the treatment of proliferative vascular diseases, including post-angioplasty restenosis and in-stent restenosis.

Declarations

COMPETING INTERESTS

The authors declare no competing interests.

ETHICAL APPROVAL

All animal experiments were approved by the Ethics Committee and the Animal Care and Use Committee of Harbin Medical University, and were performed in strict accordance with the US National Institutes of Health Guide for the Care and Use of Laboratory Animals (NIH Publication No. 85–23, revised 1996). Mice were randomly assigned to experimental groups using a computer-generated randomization procedure.

AUTHOR CONTRIBUTIONS

WP, YZ and YL conceived the study concept. CL, JL and YZ performed the animal experiments, conducted Western blot and qPCR analysis. CL, ZZ and YY performed cell culture and IF staining. SW, CY and KW performed the histological examination of mice samples. CL, JLand YZ carried out the data analysis. WP and CL wrote the manuscript. WP, YZ and DZ provided the funding. All authors reviewed the manuscript.

ACKNOWLEDGMENT

This work was supported by National Natural Science Foundation of China (82430017 to Z.P.), Young Talents Project funding of Heilongjiang Province (CYQN24041 to Y.Z.), The Key Research and Development Plan Project of Heilongjiang Province (No.2023 ZX06C13 to D.Z.) and the National Multidisciplinary Innovation Team Project in Traditional Chinese Medicine (ZYYCXTD-D-202407).

DATA AVAILABILITY

All data generated or analyzed during this study are included in the main article and its Supplementary Information. Additional data are available from the corresponding author upon reasonable request.

References

1. Cao, G., X. Xuan, J. Hu, R. Zhang, H. Jin, H. Dong, How vascular smooth muscle cell phenotype switching contributes to vascular disease. Cell Commun Signal, 2022. 20(1): p. 180.
2. Tang, H.Y., A.Q. Chen, H. Zhang, X.F. Gao, X.Q. Kong, J.J. Zhang, Vascular Smooth Muscle Cells Phenotypic Switching in Cardiovascular Diseases. Cells, 2022. 11(24).
3. Elmarasi, M., I. Elmakaty, B. Elsayed, A. Elsayed, J.A. Zein, A. Boudaka, *et al.*, Phenotypic switching of vascular smooth muscle cells in atherosclerosis, hypertension, and aortic dissection. J Cell Physiol, 2024. 239(4): p. e31200.
4. Owens, G.K., M.S. Kumar, B.R. Wamhoff, Molecular regulation of vascular smooth muscle cell differentiation in development and disease. Physiol Rev, 2004. 84(3): p. 767–801.
5. Ikedo, H., K. Tamaki, S. Ueda, S. Kato, M. Fujii, P. Ten Dijke, *et al.*, Smad protein and TGF-beta signaling in vascular smooth muscle cells. Int J Mol Med, 2003. 11(5): p. 645–50.

6. Qi, Y.X., J. Jiang, X.H. Jiang, X.D. Wang, S.Y. Ji, Y. Han, *et al.*, PDGF-BB and TGF-{beta}1 on cross-talk between endothelial and smooth muscle cells in vascular remodeling induced by low shear stress. Proc Natl Acad Sci U S A, 2011. 108(5): p. 1908–13.
7. Gong, X., Y. Liu, H. Liu, N. Cao, L. Zeng, M. Tian, *et al.*, Re-analysis of single-cell transcriptomics reveals a critical role of macrophage-like smooth muscle cells in advanced atherosclerotic plaque. Theranostics, 2024. 14(4): p. 1450–1463.
8. Wang, P., V.C. Mak, L. Rao, Q. Wu, Y. Zhou, R. Sharma, *et al.*, p85β acts as a transcription cofactor and cooperates with BCLAF1 in the nucleus. Nat Commun, 2025. 16(1): p. 2042.
9. Vohhodina, J., E.M. Barros, A.L. Savage, F.G. Liberante, L. Manti, P. Bankhead, *et al.*, The RNA processing factors THRAP3 and BCLAF1 promote the DNA damage response through selective mRNA splicing and nuclear export. Nucleic Acids Res, 2017. 45(22): p. 12816–12833.
10. Shao, A.W., H. Sun, Y. Geng, Q. Peng, P. Wang, J. Chen, *et al.*, Bclaf1 is an important NF-κB signaling transducer and C/EBPβ regulator in DNA damage-induced senescence. Cell Death Differ, 2016. 23(5): p. 865–75.
11. Zhou, X., X. Zhou, J. Li, Y. He, S. Qiu, Y. Xu, *et al.*, Bclaf1 mediates super-enhancer-driven activation of POLR2A to enhance chromatin accessibility in nitrosamine-induced esophageal carcinogenesis. J Hazard Mater, 2025. 492: p. 138218.
12. Zhang, Y., H. Gao, Y. Lu, Y. Zhang, M. Yang, X. Zhang, *et al.*, Bclaf1 drives heart failure by recruiting Srsf2 to enhance Hand2 pre-mRNA splicing and pathological hypertrophy. Nature Communications, 2026. 17(1).
13. Zhang, Y., X. Zhang, B. Cai, Y. Li, Y. Jiang, X. Fu, *et al.*, The long noncoding RNA lncCIRBIL disrupts the nuclear translocation of Bclaf1 alleviating cardiac ischemia-reperfusion injury. Nat Commun, 2021. 12(1): p. 522.
14. Sata, M., Y. Maejima, F. Adachi, K. Fukino, A. Saiura, S. Sugiura, *et al.*, A mouse model of vascular injury that induces rapid onset of medial cell apoptosis followed by reproducible neointimal hyperplasia. J Mol Cell Cardiol, 2000. 32(11): p. 2097–104.
15. Ma, Z., C. Mao, X. Chen, S. Yang, Z. Qiu, B. Yu, *et al.*, Peptide Vaccine Against ADAMTS-7 Ameliorates Atherosclerosis and Postinjury Neointima Hyperplasia. Circulation, 2023. 147(9): p. 728–742.
16. Mao, C., Z. Ma, Y. Jia, W. Li, N. Xie, G. Zhao, *et al.*, Nidogen-2 Maintains the Contractile Phenotype of Vascular Smooth Muscle Cells and Prevents Neointima Formation via Bridging Jagged1-Notch3 Signaling. Circulation, 2021. 144(15): p. 1244–1261.
17. Chen, R., D.G. McVey, D. Shen, X. Huang, S. Ye, Phenotypic Switching of Vascular Smooth Muscle Cells in Atherosclerosis. J Am Heart Assoc, 2023. 12(20): p. e031121.
18. Li, J., X. Li, S. Song, Z. Sun, Y. Li, L. Yang, *et al.*, Mitochondria spatially and temporally modulate VSMC phenotypes via interacting with cytoskeleton in cardiovascular diseases. Redox Biol, 2023. 64: p. 102778.
19. Hubert, M.O., J. Rodriguez-Vita, L. Wiedmann, A. Fischer, Isolation of Murine Primary Aortic Smooth Muscle Cells. Bio Protoc, 2021. 11(3): p. e3907.

20. Grootaert, M.O.J., M.R. Bennett, Vascular smooth muscle cells in atherosclerosis: time for a re-assessment. Cardiovasc Res, 2021. 117(11): p. 2326–2339.
21. Jia, Y., C. Mao, Z. Ma, J. Huang, W. Li, X. Ma, *et al.*, PHB2 Maintains the Contractile Phenotype of VSMCs by Counteracting PKM2 Splicing. Circ Res, 2022. 131(10): p. 807–824.
22. Zhao, G., H. Lu, Z. Chang, Y. Zhao, T. Zhu, L. Chang, *et al.*, Single-cell RNA sequencing reveals the cellular heterogeneity of aneurysmal infrarenal abdominal aorta. Cardiovasc Res, 2021. 117(5): p. 1402–1416.
23. Dominguez, R., K.C. Holmes, Actin structure and function. Annu Rev Biophys, 2011. 40: p. 169–86.
24. Tang, D.D., Y. Anfinogenova, Physiologic properties and regulation of the actin cytoskeleton in vascular smooth muscle. J Cardiovasc Pharmacol Ther, 2008. 13(2): p. 130–40.
25. Radine, C., D. Peters, A. Reese, J. Neuwahl, W. Budach, R.U. Jänicke, *et al.*, The RNA-binding protein RBM47 is a novel regulator of cell fate decisions by transcriptionally controlling the p53-p21-axis. Cell Death Differ, 2020. 27(4): p. 1274–1285.
26. Shao, A., Y. Lang, M. Wang, C. Qin, Y. Kuang, Y. Mei, *et al.*, Bclaf1 is a direct target of HIF-1 and critically regulates the stability of HIF-1α under hypoxia. Oncogene, 2020. 39(13): p. 2807–2818.
27. Zhou, Y., X. Ran, M. Han, BCLAF1 is Expressed as a Potential Anti-oncogene in Bile Duct Cancer. Biochemical Genetics, 2024. 62(5): p. 3681–3694.
28. Wen, Y., X. Zhou, M. Lu, M. He, Y. Tian, L. Liu, *et al.*, Bclaf1 promotes angiogenesis by regulating HIF-1α transcription in hepatocellular carcinoma. Oncogene, 2018. 38(11): p. 1845–1859.
29. Davis, M.J., S. Earley, Y.S. Li, S. Chien, Vascular mechanotransduction. Physiol Rev, 2023. 103(2): p. 1247–1421.
30. Shao, Y., L. Yi, Q. Zhu, Y. Zhou, T. Chen, W. Yao, Ginkgolic Acid Inhibits VSMC Proliferation and Migration and Vascular Restenosis by Regulating Cell Cycle Progression and Cytoskeleton Rearrangement Through TCTN1. Cells, 2025. 14(23).
31. Wang, G., L. Jacquet, E. Karamariti, Q. Xu, Origin and differentiation of vascular smooth muscle cells. J Physiol, 2015. 593(14): p. 3013–30.
32. Goel, S.A., L.W. Guo, B. Liu, K.C. Kent, Mechanisms of post-intervention arterial remodelling. Cardiovasc Res, 2012. 96(3): p. 363–71.
33. Rzucidlo, E.M., K.A. Martin, R.J. Powell, Regulation of vascular smooth muscle cell differentiation. J Vasc Surg, 2007. 45 Suppl A: p. A25-32.
34. Hu, Y., Z. Cai, B. He, Smooth Muscle Heterogeneity and Plasticity in Health and Aortic Aneurysmal Disease. Int J Mol Sci, 2023. 24(14).
35. Basatemur, G.L., H.F. Jørgensen, M.C.H. Clarke, M.R. Bennett, Z. Mallat, Vascular smooth muscle cells in atherosclerosis. Nat Rev Cardiol, 2019. 16(12): p. 727–744.
36. Zhu, N., Z.F. Guo, K. Kazama, B. Yi, N. Tongmuang, H. Yao, *et al.*, Epigenetic regulation of vascular smooth muscle cell phenotypic switch and neointimal formation by PRMT5. Cardiovasc Res, 2023. 119(12): p. 2244–2255.

37. Rykaczewska, U., Q. Zhao, P. Saliba-Gustafsson, M. Lengquist, M. Kronqvist, O. Bergman, *et al.*, Plaque Evaluation by Ultrasound and Transcriptomics Reveals BCLAF1 as a Regulator of Smooth Muscle Cell Lipid Transdifferentiation in Atherosclerosis. Arterioscler Thromb Vasc Biol, 2022. 42(5): p. 659–676.
38. Kasof, G.M., L. Goyal, E. White, Btf, a novel death-promoting transcriptional repressor that interacts with Bcl-2-related proteins. Mol Cell Biol, 1999. 19(6): p. 4390–404.
39. Lee, S.H., R.F. Kalejta, J. Kerry, O.J. Semmes, C.M. O'Connor, Z. Khan, *et al.*, BclAF1 restriction factor is neutralized by proteasomal degradation and microRNA repression during human cytomegalovirus infection. Proc Natl Acad Sci U S A, 2012. 109(24): p. 9575–80.
40. Tang, D.D., B.D. Gerlach, The roles and regulation of the actin cytoskeleton, intermediate filaments and microtubules in smooth muscle cell migration. Respir Res, 2017. 18(1): p. 54.
41. Vartiainen, M.K., S. Guettler, B. Larijani, R. Treisman, Nuclear actin regulates dynamic subcellular localization and activity of the SRF cofactor MAL. Science, 2007. 316(5832): p. 1749–52.
42. Wang, W., W. Zhang, Y. Han, J. Chen, Y. Wang, Z. Zhang, *et al.*, NELIN, a new F-actin associated protein, stimulates HeLa cell migration and adhesion. Biochem Biophys Res Commun, 2005. 330(4): p. 1127–31.
43. Kaplan-Albuquerque, N., Y.E. Bogaert, V. Van Putten, M.C. Weiser-Evans, R.A. Nemenoff, Patterns of gene expression differentially regulated by platelet-derived growth factor and hypertrophic stimuli in vascular smooth muscle cells: markers for phenotypic modulation and response to injury. J Biol Chem, 2005. 280(20): p. 19966–76.
44. Lin, Z., C. Wang, Z. Wen, Z. Cai, W. Guo, X. Feng, *et al.*, NEXN regulates vascular smooth muscle cell phenotypic switching and neointimal hyperplasia. JCI Insight, 2025. 10(13).
45. Engeland, K., Cell cycle regulation: p53-p21-RB signaling. Cell Death Differ, 2022. 29(5): p. 946–960.
46. Chang, M.W., E. Barr, M.M. Lu, K. Barton, J.M. Leiden, Adenovirus-mediated over-expression of the cyclin/cyclin-dependent kinase inhibitor, p21 inhibits vascular smooth muscle cell proliferation and neointima formation in the rat carotid artery model of balloon angioplasty. J Clin Invest, 1995. 96(5): p. 2260–8.

Figures

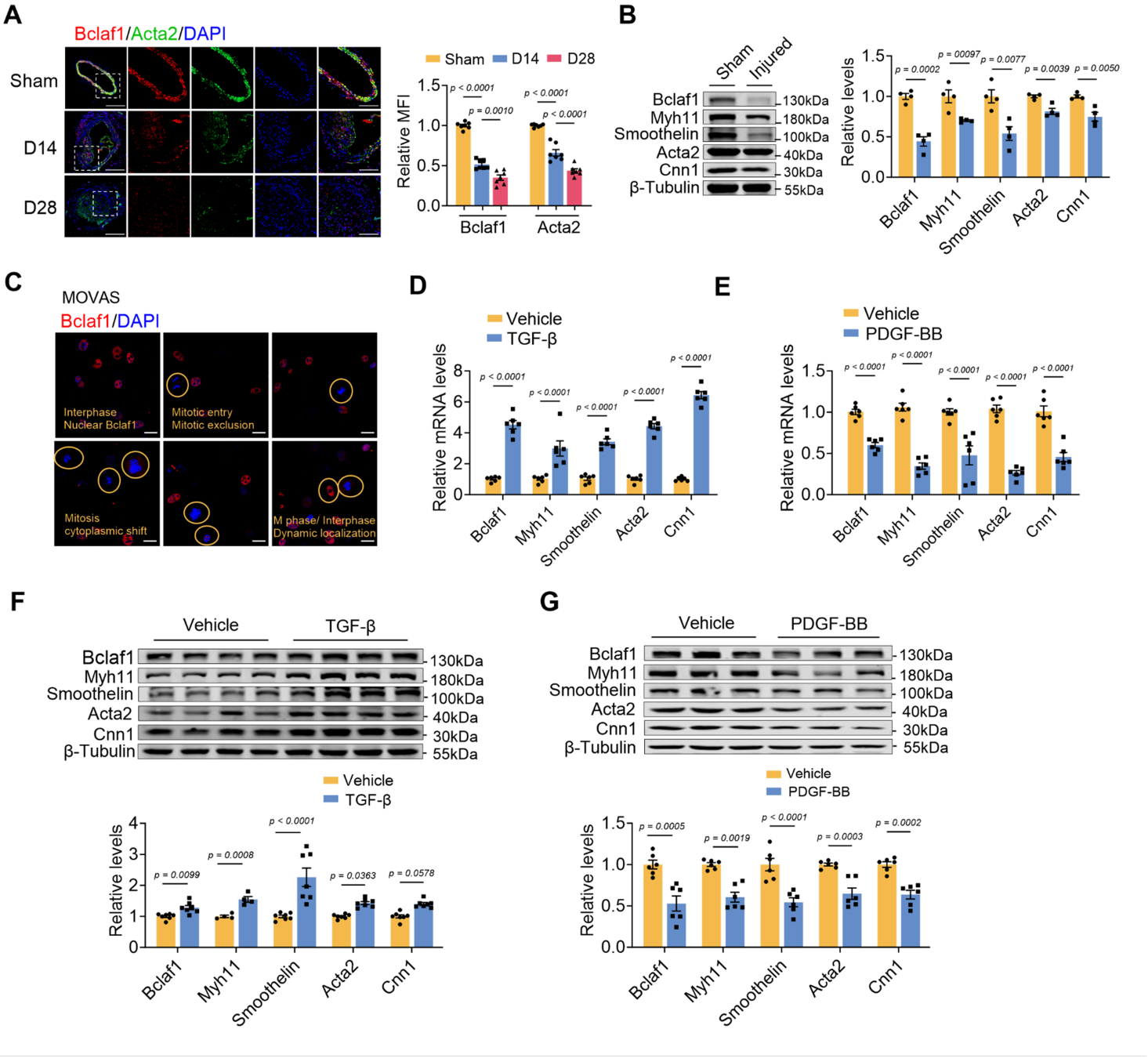


Figure 1

Bclaf1 is downregulated during vascular smooth muscle cell phenotypic transition and vascular injury.

A, Immunofluorescent staining for Bclaf1 (red), Acta2 (green), and DAPI (blue) in carotid arteries from 10-week-old male WT mice at days 14 and 28 after surgery, with sham operated arteries as controls. Scale bar = 50 μm. **Right**, Quantification of the relative MFI of Bclaf1 and Acta2. N=6. **B,** Western blot analysis and quantification of Bclaf1 and contractile VSMC markers Myh11, Smoothelin, Acta2 and Cnn1 in sham and injured carotid arteries. N=4, with each replicate derived from pooled carotid artery tissues from 3 mice. **C**, Representative immunofluorescence images showing cell cycle-dependent subcellular localization of Bclaf1 in VSMCs. Bclaf1 was predominantly localized in the nucleus during interphase,

enriched at replication foci during S phase, and excluded from condensed chromosomes with cytoplasmic redistribution during mitosis. Yellow circles indicate mitotic cells. Scale bar, 50 μm. **D**, qRT-PCR analysis of Bclaf1 and contractile VSMC markers (Myh11, Smoothelin, Acta2, Cnn1) in MOVAS cells treated with TGF-β (10 μg/L) for 24 h. N=6. **E**, qRT-PCR analysis of Bclaf1 and contractile VSMC markers (Myh11, Smoothelin, Acta2, Cnn1) in serum-starved MOVAS cells stimulated with PDGF-BB (20 μg/L) for 24 h. N=6. **F**, Representative Western blot and quantifications of Bclaf1 and contractile VSMC markers (Myh11, Smoothelin, Acta2, Cnn1) in MOVAS cells treated with TGF-β (10 μg/L) for 48 h. β-Tubulin was used as a loading control. N=7. **G**, Representative Western blot and quantifications of Bclaf1 and contractile VSMC markers (Myh11, Smoothelin, Acta2, Cnn1) in serum-starved MOVAS cells stimulated with PDGF-BB (20 μg/L) for 48 h. β-Tubulin was used as a loading control. N=7. All quantitative data are presented as the mean ± standard error of the mean (Mean ± SEM). Data were analyzed using two-tailed unpaired Student's t-tests. One-way ANOVA was used to determine difference among different time points. MOVAS indicates Mouse Aortic Vascular Smooth Muscle cells; WT, wild-type; MFI, mean fluorescence intensity.

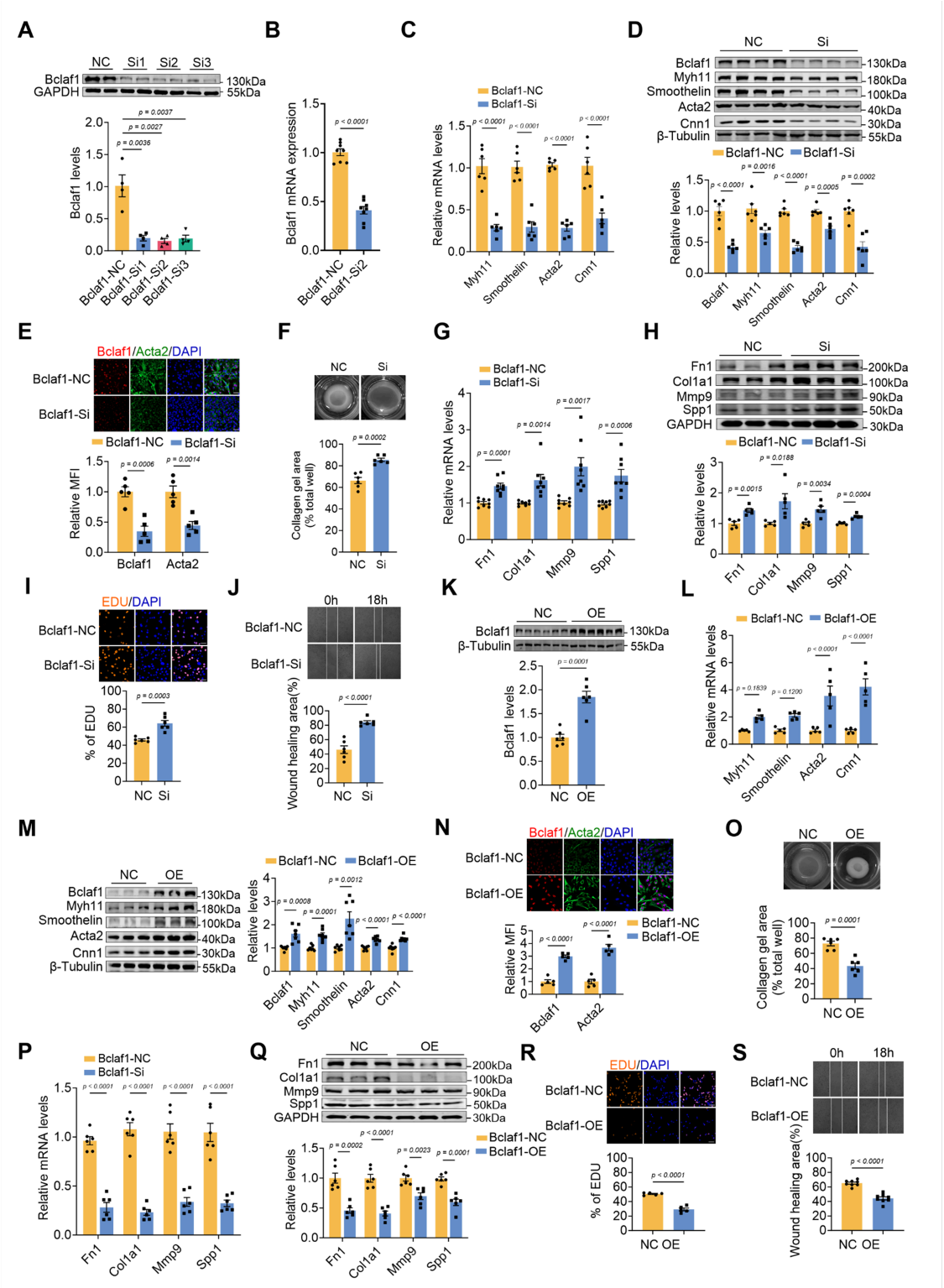


Figure 2

Bclaf1 regulates vascular smooth muscle cell phenotypic switching.

A, Representative Western blot and quantification of Bclaf1 protein levels in MOVAS transfected with si-Bclaf1 (Si1, Si2, Si3) or negative control siRNA (NC). β-Tubulin was used as the loading control. N=6. **B**, qRT-PCR analysis of Bclaf1 mRNA expression in MOVAS transfected with Bclaf1-NC or Bclaf1-Si. N=8. **C**,

qRT-PCR analysis of contractile VSMC markers (Myh11, Smoothelin, Acta2, Cnn1) in MOVAS transfected with Bclaf1-NC or Bclaf1-Si. N=6. **D**, Representative Western blot and quantification of the expression of Bclaf1 and VSMC contractile proteins (Myh11, Smoothelin, Acta2, Cnn1) in MOVAS transfected with negative control siRNA (Bclaf1-NC) or Bclaf1 siRNA (Bclaf1-Si). β-Tubulin was used as a loading control. N=6. **E**, Representative immunofluorescence images of Bclaf1 (red), Acta2 (green), and DAPI (blue) in MOVAS transfected with Bclaf1-NC or Bclaf1-Si. Scale bar=50 μm. **Bottom**, Quantification of MFI of Bclaf1 and Acta2. N=5. **F**, Representative images and quantitative analysis of the collagen gel contraction assay. MOVAS were transfected with Bclaf1-NC or Bclaf1-Si for 48 hours. Then the cells were harvested and mixed with ice-cold collagen gel solution at a volume ratio of 1:4. Twenty-four hours after collagen polymerization, the size of the collagen gel in each well was evaluated. N=6 for each group. **G**, qRT-PCR analysis of synthetic VSMC markers (Fn1, Col1a1, Mmp9, Spp1) in MOVAS transfected with Bclaf1-NC or Bclaf1-Si. N=8. **H**, Representative Western blot and quantification of synthetic VSMC proteins (Fn1, Col1a1, Mmp9, Spp1) in MOVAS transfected with Bclaf1-NC or Bclaf1-Si. GAPDH was used as a loading control. N=5. **I**, Representative immunofluorescent images of EDU (orange) and DAPI (blue) staining in MOVAS transfected with Bclaf1-NC or Bclaf1-Si. Scale bar=50 μm. **Bottom**, Quantification of the percentage of EDU-positive cells. N=6. **J**, Representative images and quantitative analysis of the wound-healing assay. Confluent MOVAS were transfected with Bclaf1-NC or Bclaf1-Si and subjected to a scratch-wound assay. Images were taken at 0 and 18 hours after scratching (the white lines indicate the wound edges). N=6. **K**, Representative Western blot and quantification of Bclaf1 protein levels in MOVAS transfected with Bclaf1 overexpression plasmid (OE) or empty vector control (NC). β-Tubulin was used as the loading control. N=6. **L**, qRT-PCR analysis of contractile VSMC markers (Myh11, Smoothelin, Acta2, Cnn1) in MOVAS transfected with Bclaf1-NC or Bclaf1-OE. N=6. **M**, Representative Western blot and quantification of Bclaf1 and VSMC contractile proteins (Myh11, Smoothelin, Acta2, Cnn1) in MOVAS transfected with negative control vector (Bclaf1-NC) or Bclaf1 overexpression plasmid (Bclaf1-OE). β-Tubulin was used as a loading control. N=6. **N**, Representative immunofluorescence images of Bclaf1 (red), Acta2 (green), and DAPI (blue) in MOVAS transfected with Bclaf1-NC or Bclaf1-OE. Scale bar=50 μm. **Bottom**, Quantification of MFI of Bclaf1 and Acta2. N=5. **O**, Representative images and quantitative analysis of the collagen gel contraction assay. MOVAS were transfected with Bclaf1-NC or Bclaf1-OE for 48 hours. Then the cells were harvested and mixed with ice-cold collagen gel solution at a volume ratio of 1:4. Twenty-four hours after collagen polymerization, the size of the collagen gel in each well was evaluated. N=6. **P**, qRT-PCR analysis of synthetic VSMC markers (Fn1, Col1a1, Mmp9, Spp1) in MOVAS transfected with Bclaf1-NC or Bclaf1-OE. N=6. **Q**, Representative Western blot and quantification of synthetic VSMC proteins (Fn1, Col1a1, Mmp9, Spp1) in MOVAS transfected with Bclaf1-NC or Bclaf1-OE. GAPDH was used as a loading control. N=6. **R**, Representative immunofluorescent images of EDU (orange) and DAPI (blue) staining in MOVAS transfected with Bclaf1-NC or Bclaf1-OE. Scale bar=50 μm. **Bottom**, Quantification of the percentage of EDU positive cells. N=6. **S**, Representative images and quantitative analysis of the wound healing assay. Confluent MOVAS were transfected with Bclaf1-NC or Bclaf1-OE and subjected to a scratch-wound assay. Images were taken at 0 and 18 hours after scratching. N=8. All quantitative data are presented as Mean ± SEM. Data were analyzed using two-tailed unpaired Student's t-tests.

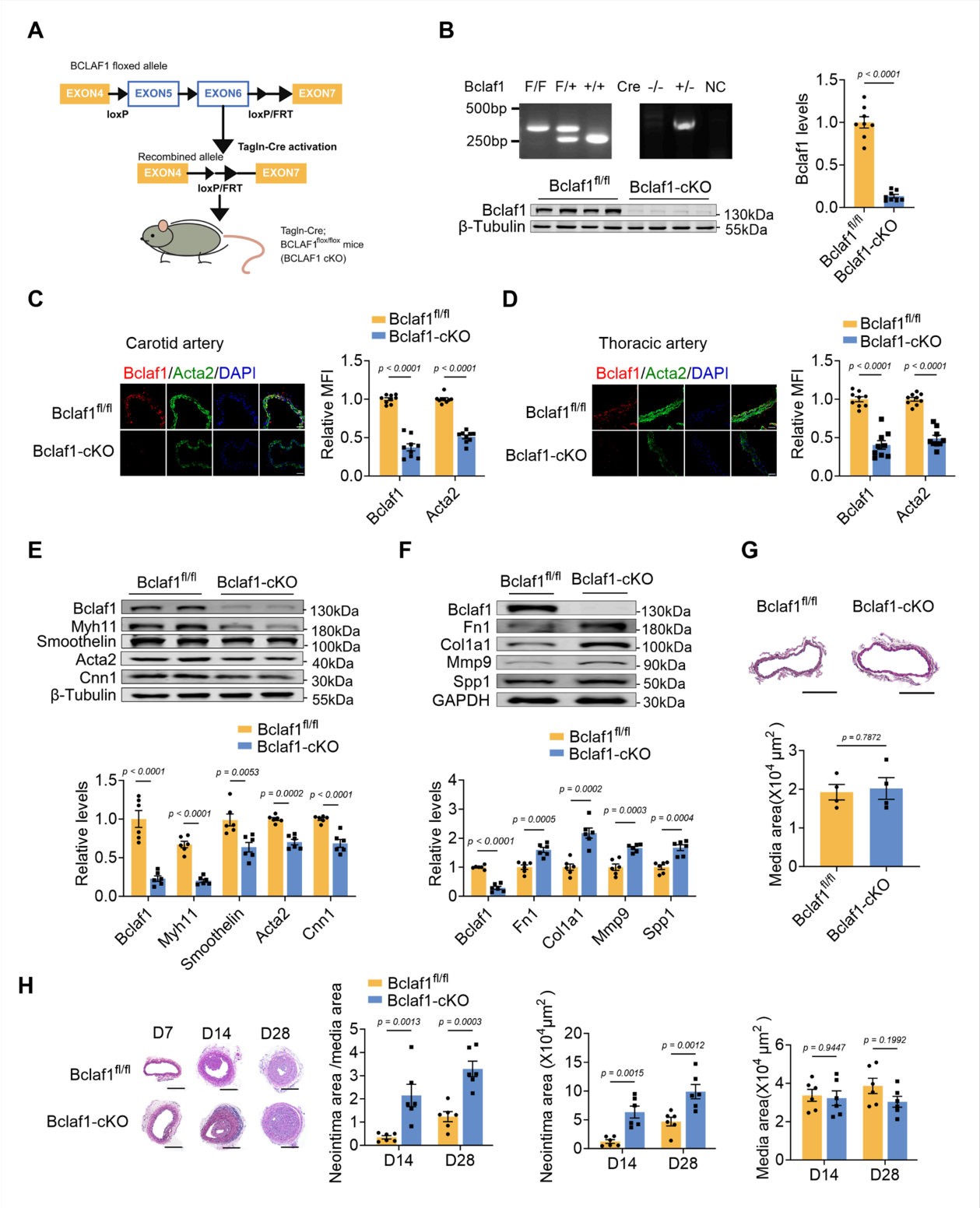


Figure 3

Bclaf1 deficiency exacerbates post-injury neointima formation *in vivo*.

A, Schematic diagram for the generation of smooth muscle cell-specific Bclaf1 cKO mice using TagIn-Cre. **B**, Representative Western blot and quantification of Bclaf1 expression in the arteries of *Bclaf1*$^{fl/fl}$ and *Bclaf1* cKO mice. β-Tubulin was used as a loading control. N=8. **C**, Representative

immunofluorescence images of Bclaf1 (red), Acta2 (green), and DAPI (blue) in the carotid arteries of *Bclaf1*$^{fl/fl}$ and *Bclaf1* cKO mice. Scale bar=50 μm. **Right**, Quantification of the relative MFI of Bclaf1 and Acta2. N=9. **D**, Representative immunofluorescent images of Bclaf1 (red), Acta2 (green), and DAPI (blue) in the thoracic arteries of *Bclaf1*$^{fl/fl}$ and *Bclaf1* cKO mice. Scale bar=50 μm. **Right**, Quantification of the relative MFI of Bclaf1 and Acta2. N=9. **E**, Representative Western blot and quantification of Bclaf1 and VSMC contractile proteins (Myh11, Smoothelin, Acta2, Cnn1) in aortas from *Bclaf1*$^{fl/fl}$ and *Bclaf1* cKO mice. β-Tubulin was used as a loading control. N=6. **F**, Representative Western blot and quantification of synthetic VSMC proteins (Fn1, Col1a1, Mmp9, Spp1) in aortas of *Bclaf1*$^{fl/fl}$ and *Bclaf1* cKO mice. GAPDH was used as a loading control. N=6. **G**, Representative cross-sections of hematoxylin and eosin(H&E) stained thoracic arteries of *Bclaf1*$^{fl/fl}$ and *Bclaf1* cKO mice under baseline conditions. Scale bar=200 μm. **Right**, Quantitative analysis of the media area in histological sections. N=6. **H**, Representative cross-sections of H&E stained carotid arteries of *Bclaf1*$^{fl/fl}$ and *Bclaf1* cKO mice at days 14, and 28 after ligation. Scale bar=200 μm. **Right**, Quantitative analysis of the neointima area, neointima to media area ratio, and media area in histological sections from ligated carotid arteries of *Bclaf1*$^{fl/fl}$ and *Bclaf1*cKO mice at days 14 and 28. N=6. p-values obtained via two-tailed unpaired Student's t-tests. Two-way ANOVA followed by Tukey's test was used to determine the difference among various time points. cKO indicates conditional knockout.

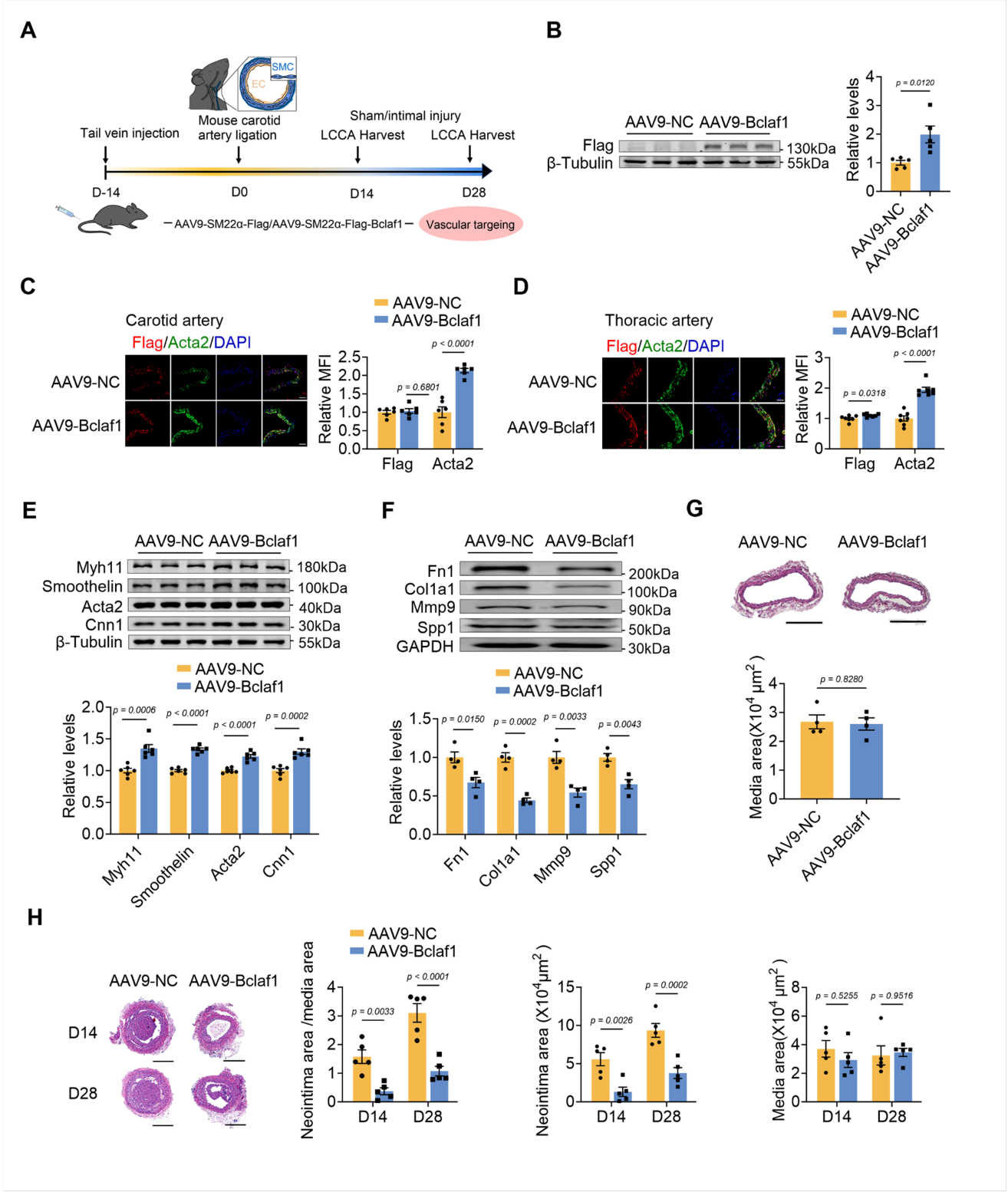


Figure 4

Smooth muscle cell-specific overexpression of Bclaf1 via AAV9 inhibits post-injury neointima formation in mice.

A, The simple schematic diagram for the construction of smooth muscle cell-specific AAV9-Bclaf1 recombinant virus. **B**, Representative Western blot and quantification of Flag-tagged Bclaf1 expression in

the arteries of WT mice injected with AAV9-NC or AAV9-Bclaf1. β-Tubulin was used as a loading control. N=5. **C**, Representative immunofluorescence images of Flag-tagged Bclaf1 (red), Acta2 (green), and DAPI (blue) in the carotid arteries of WT mice injected with AAV9-NC or AAV9-Bclaf1. Scale bar=50 μm. **Right**, Quantification of the relative MFI of Flag-tagged Bclaf1 and Acta2. N=6. **D**, Representative immunofluorescence images of Flag (red), Acta2 (green), and DAPI (blue) in the thoracic arteries of WT mice injected with AAV9-NC or AAV9-Bclaf1. Scale bar=50 μm. Right, Quantification of the relative MFI of Flag and Acta2. n=7. **E**, Representative Western blot and quantification of VSMC contractile proteins (Myh11, Smoothelin, Acta2, Cnn1) in aortas from WT mice injected with AAV9-NC or AAV9-Bclaf1. β-Tubulin was used as a loading control. N=6. **F**, Representative Western blot and quantification of synthetic VSMC proteins (Fn1, Col1a1, Mmp9, Spp1) in aortas from WT mice injected with AAV9-NC or AAV9-Bclaf1. GAPDH was used as a loading control. N=6. **G**, Representative cross-sections of hematoxylin and eosin–stained thoracic arteries of WT mice injected with AAV9-NC or AAV9-Bclaf1 under baseline conditions. Scale bar=200 μm. **Right**, Quantitative analysis of the media area in histological sections. N=4. **H**, Representative cross-sections of hematoxylin and eosin–stained carotid arteries of WT mice injected with AAV9-NC or AAV9-Bclaf1 at days 14 and 28 after ligation. Scale bar=200 μm. **Right**, Quantitative analysis of the neointima area, neointima-to-media area ratio, and media area in histological sections from ligated carotid arteries of WT mice injected with AAV9-NC or AAV9-Bclaf1 at days 14 and 28. n=5. p-values obtained via two-tailed unpaired Student's t-tests. Two-way ANOVA followed by Tukey's test was used to determine the difference among various time points. AAV9, adeno-associated virus serotype 9.

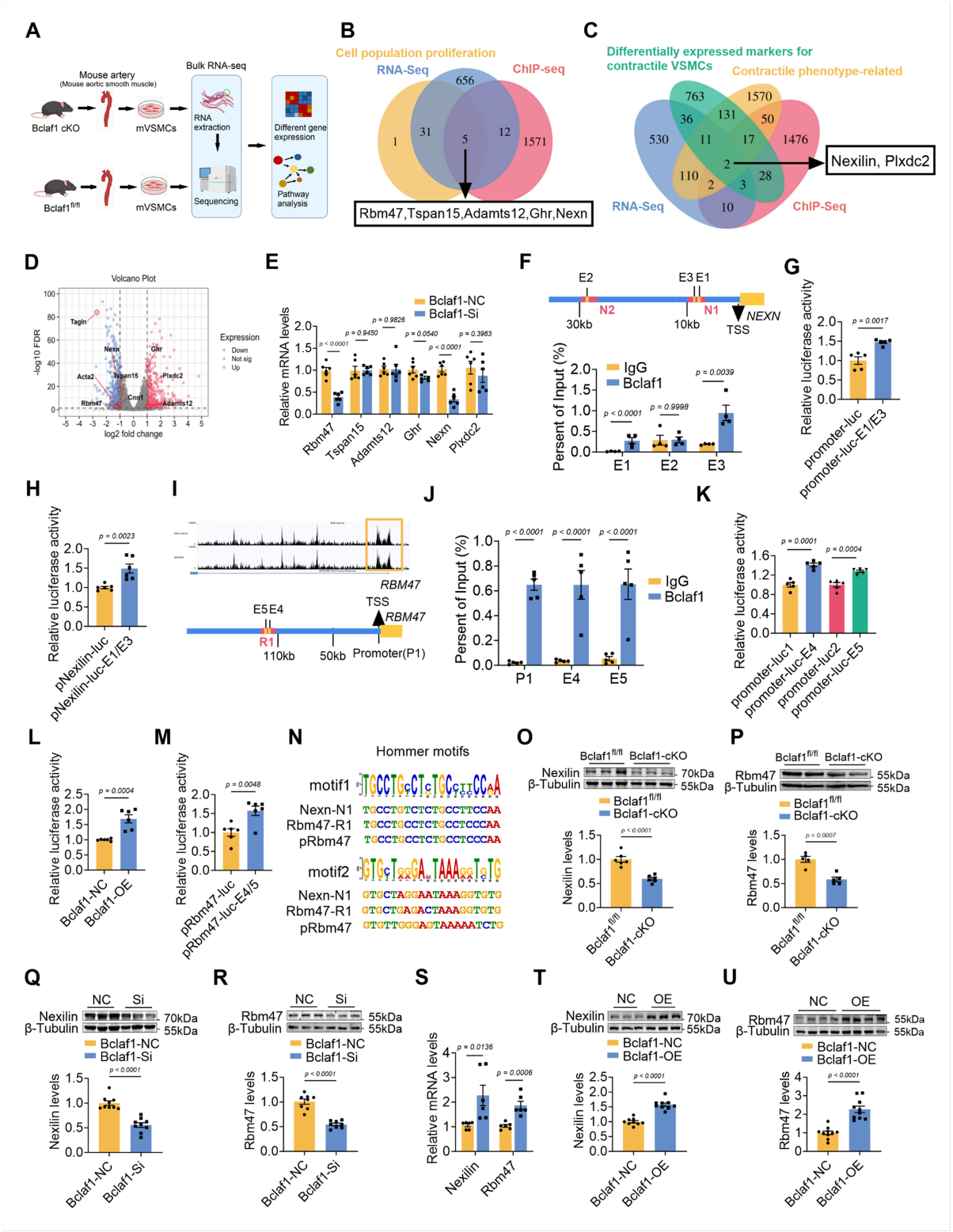


Figure 5

Bclaf1 regulates the transcriptome in vascular smooth muscle cell.

A, Schematic diagram of the RNA sequencing workflow in mVSMCs isolated from Bclaf1$^{fl/fl}$ and Bclaf1 cKO mice. **B**, Venn diagram depicting the overlap between DEGs and Bclaf1 ChIP-seq target genes, highlighting key target genes related to cell population proliferation (Rbm47, Tspan15, Adamts15, Ghr,

Nexn). **C**, Venn diagram depicting the overlap between DEGs and Bclaf1 ChIP-seq target genes, highlighting key target genes related to VSMCs contractile phenotype-related genes (Plxdc2, Nexilin). **D**, qRT-PCR validation of *Rbm47, Tspan15, Adamts12, Ghr, Nexn, Plxdc2* mRNA levels in MOVAS cells transfected with Bclaf1-NC or Bclaf1-Si. **E**, Volcano plot showing differentially expressed genes (DEGs) between Bclaf1$^{fl/fl}$ and Bclaf1 cKO groups. Gray dots indicate genes with no significant change. **F**, Schematic diagram of the Bclaf1 binding loci in the genomic regions of *Nexn,* and ChIP-qPCR validation of Bclaf1 binding to *Nexn* predicted regions in MOVAS, with IgG as a negative control. **G**, Dual-luciferase reporter assay showing the enhancer activity of *Nexn* E1/E3 fragment in MOVAS. N=5 per group. **H**, Relative luciferase reporter activities normalized to the *Nexn* promoter-luc plasmid. N=5 per group. **I**, Representative ChIP-seq tracks from the Cistrome Data Browser showing Bclaf1 binding peak at the *Rbm47* promoter region and Schematic diagram of the Bclaf1 binding loci in the genomic regions of *Rbm47*. **J**, ChIP-qPCR validation of Bclaf1 binding to *Rbm47* predicted regions in MOVAS, with IgG as a negative control. **K**, Dual-luciferase reporter assay showing the enhancer activity of *Rbm47* E4 and E5 fragments in MOVAS. N=5 per group. **L**, Dual-luciferase reporter assay showing the luciferase activity of Rbm47 promoter driven by Bclaf1-NC or Bclaf1-OE in MOVAS. N=6 per group. **M**, Relative luciferase reporter activities normalized to *Rbm47* promoter-luc plasmid. N=5 per group. **N**, MEME Suite motif analysis identifying consensus Bclaf1 binding sequences in Rbm47 promoter, Rbm47 enhancer and Nexn enhancer regions. **O**, Representative Western blot and quantitative analysis of Nexilin protein levels in Bclaf1$^{fl/fl}$ and Bclaf1 cKO mice. β-Tubulin was used as a loading control. N=6 per group. **P**, Representative Western blot and quantitative analysis of Rbm47 protein levels in Bclaf1$^{fl/fl}$ and Bclaf1 cKO mice. β-Tubulin was used as a loading control. N=5 per group. **Q**, Representative Western blot and quantitative analysis of Nexilin protein levels in Bclaf1-Si and Bclaf1-NC MOVAS. β-Tubulin was used as a loading control. N=9 per group. **R,** Representative Western blot and quantitative analysis of Rbm47 protein levels in Bclaf1-Si and Bclaf1-NC MOVAS. β-Tubulin was used as a loading control. N=8 per group. **S**, qRT-PCR analysis of Nexn and Rbm47 mRNA expression levels in Bclaf1-OE and Bclaf1-NC MOVAS. N= 6 per group. **T**, Representative Western blot and quantitative analysis of Bclaf1 and Nexilin protein levels in Bclaf1-OE and Bclaf1-NC MOVAS. β-Tubulin was used as a loading control. N=9 per group. **U**, Representative Western blot and quantitative analysis of Rbm47 protein levels in Bclaf1-OE and Bclaf1-NC MOVAS. β-Tubulin was used as a loading control. N=10 per group. All quantitative data are presented as Mean ± SEM. Data were analyzed using two-tailed unpaired Student’s t-tests.

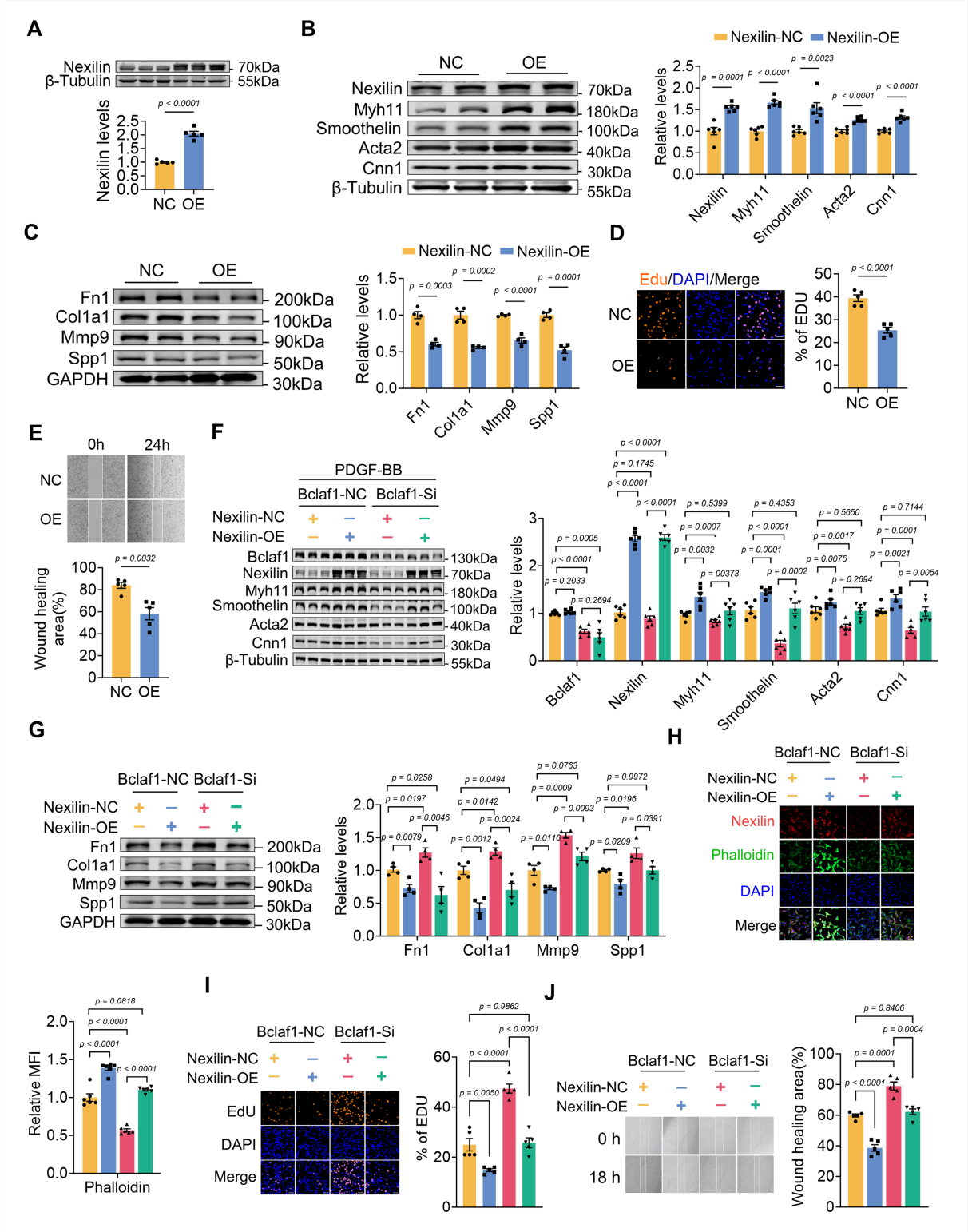


Figure 6

Nexilin mediates the effects of Bclaf1 on vascular smooth muscle cell contractile phenotype and proliferation.

A, Representative Western blot and quantification of Nexilin levels in MOVAS transfected with Nexilin OE or NC. β-Tubulin was used as the loading control. N=5 per group. **B**, Representative Western blot and

quantification of Nexilin and VSMC contractile proteins (Myh11, Smoothelin, Acta2, Cnn1) in Nexilin-NC and Nexilin-OE MOVAS. β-Tubulin was used as a loading control. N=6. **C**, Representative Western blot and quantification of synthetic VSMC proteins (Fn1, Col1a1, Mmp9, Spp1) in Nexilin-NC and Nexilin-OE MOVAS. GAPDH was used as the loading control. N=4. **D**, Representative EdU staining images (EdU, orange; DAPI, blue) and quantification of EdU-positive cells in Nexilin-NC and Nexilin-OE MOVAS. Scale bar=50 μm. N=5 per group. **E**, Representative images and quantitative analysis of wound-healing assay in Nexilin-NC and Nexilin-OE MOVAS. Images were taken at 0 and 24 hours after scratching. N=5 per group. **F**, Representative Western blot and quantification of Bclaf1, Nexilin, and VSMC contractile proteins (Myh11, Smoothelin, Acta2, Cnn1) in MOVAS transfected with Bclaf1-NC or Bclaf1-Si, with or without Nexilin overexpression, followed by PDGF-BB (20 μg/L) treatment for 48 h. β-Tubulin was used as the loading control. N=6. **G**, Representative Western blot and quantification of synthetic VSMC proteins (Fn1, Col1a1, Mmp9, Spp1) in MOVAS transfected with Bclaf1-NC or Bclaf1-Si, with or without Nexilin overexpression. GAPDH was used as the loading control. N=4. **H**, Representative immunofluorescence images of Nexilin (red), Phalloidin (green), and DAPI (blue) in MOVAS with Bclaf1 knockdown and/or Nexilin overexpression. Scale bar=50 μm. **Right**, Quantification of the relative MFI of Nexilin and Phalloidin. N=6. **I**, Representative images and quantitative analysis of wound healing assay in MOVAS with Bclaf1 knockdown, with or without Nexilin overexpression. Images were taken at 0 and 18 hours after scratching. N=5. **J**, Representative EdU staining images (EdU, orange; DAPI, blue) and quantification of EdU-positive cells in MOVAS treated with Bclaf1-NC or Bclaf1-Si, with or without Nexilin overexpression. Scale bar=50 μm. N=5. All quantitative data are presented as Mean ± SEM. Data were analyzed using two-tailed unpaired Student’s t-tests and two-way ANOVA.

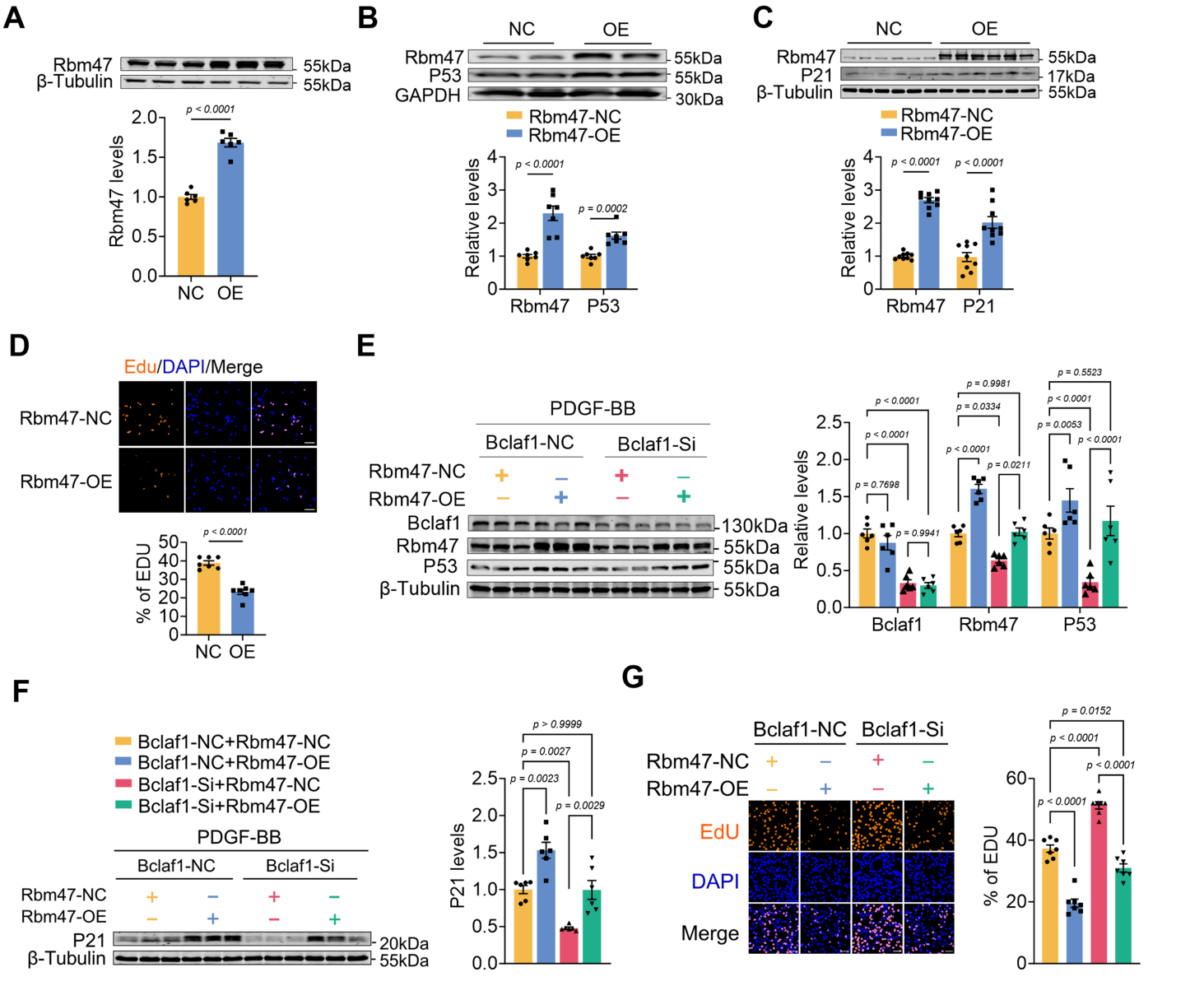


Figure 7

Rbm47 mediates the effects of Bclaf1 on vascular smooth muscle cell proliferation.

A, Representative Western blot and quantification of Rbm47 levels in MOVAS transfected with Rbm47 OE or NC. β-Tubulin was used as the loading control. N=6. **B**, Representative Western blot and quantitative analysis of Rbm47 and P53 protein levels in Rbm47-OE and Rbm47-NC MOVAS. GAPDH was used as a loading control. N=7. **C**, Representative Western blot and quantitative analysis of Rbm47 and P21 protein levels in Rbm47-OE and Rbm47-NC MOVAS. β-Tubulin was used as a loading control. N=8 per group. **D**, Representative EdU staining images (EdU, orange; DAPI, blue) and quantification of EdU positive cells in Rbm47-NC and Rbm47-OE MOVAS. Scale bar=50 μm. N=7. **E**, Representative Western blot and quantitative analysis of Bclaf1, Rbm47, and P53 protein levels in MOVAS treated with siRNA-NC or siRNA-Bclaf1, with or without Rbm47 overexpression, followed by PDGF-BB (20 μg/L) treatment for 48

hours. β-Tubulin was used as a loading control. N=6. **F**, Representative Western blot and quantitative analysis of Rbm47 and P21 protein levels in MOVAS treated with siRNA-NC or siRNA-Bclaf1, with or without Rbm47 overexpression, followed by PDGF-BB (20 μg/L) treatment for 48 hours. β-Tubulin was used as a loading control. N=6. **G**, Representative EdU staining images (EdU, orange; DAPI, blue) and quantification of EdU-positive cells in MOVAS treated with Bclaf1-NC or Bclaf1-Si, with or without Rbm47 overexpression. Scale bar=50 μm. N=7. All quantitative data are presented as Mean ± SEM. Data were analyzed using two-tailed unpaired Student's t-tests and two-way ANOVA.

Supplementary Files

This is a list of supplementary files associated with this preprint. Click to download.

- Supplementalgel.docx
- SupplementaryFigure1.tif
- SupplementaryFigure2.tif
- SupplementaryFigure3.tif
- SupplementaryFigure4.tif
- SupplementaryFigure5.tif
- SupplementaryFigure6.tif
- SupplementaryInformation.docx